Snieder, R., Sens-Schönfelder, C., Wu, R. (2017): The time dependence of rock healing as a universal relaxation process, a tutorial. - *Geophysical Journal International*, *208*, 1, pp. 1—9.

DOI: http://doi.org/10.1093/gji/ggw377

Geophysical Journal International

Geophys. J. Int. (2017) **208,** 1–9
Advance Access publication 2016 October 5
GJI Seismology

doi: 10.1093/gji/ggw377

The time dependence of rock healing as a universal relaxation process, a tutorial

Roel Snieder,[1,2] Christoph Sens-Schönfelder[2] and Renjie Wu[1]

[1] *Center for Wave Phenomena and Department of Geophysics, Colorado School of Mines, Golden, CO* 80401*, USA. E-mail: rsnieder@mines.edu*
[2] *GFZ German Research Centre for Geosciences, Potsdam, Germany*

Accepted 2016 October 4. Received 2016 September 30; in original form 2016 May 3; Editorial Decision 2016 October 3

SUMMARY

The material properties of earth materials often change after the material has been perturbed (slow dynamics). For example, the seismic velocity of subsurface materials changes after earthquakes, and granular materials compact after being shaken. Such relaxation processes are associated by observables that change logarithmically with time. Since the logarithm diverges for short and long times, the relaxation can, strictly speaking, not have a log-time dependence. We present a self-contained description of a relaxation function that consists of a superposition of decaying exponentials that has log-time behaviour for intermediate times, but converges to zero for long times, and is finite for $t = 0$. The relaxation function depends on two parameters, the minimum and maximum relaxation time. These parameters can, in principle, be extracted from the observed relaxation. As an example, we present a crude model of a fracture that is closing under an external stress. Although the fracture model violates some of the assumptions on which the relaxation function is based, it follows the relaxation function well. We provide qualitative arguments that the relaxation process, just like the Gutenberg–Richter law, is applicable to a wide range of systems and has universal properties.

Key words: Elasticity and anelasticity; Acoustic properties.

1 INTRODUCTION

The properties of rocks depend on many variables that include pressure, temperature, and moisture content. Laboratory studies (Ten Cate & Shankland 1996; Zaitsev *et al.* 2003; Vakhnenko *et al.* 2004; Ten Cate 2011) and seismological field observations (Poupinet *et al.* 1984; Schaff & Beroza 2004; Wegler & Sens-Schönfelder 2007; Brenguier *et al.* 2008; Wu *et al.* 2009; Nakata & Snieder 2011; Hobiger *et al.* 2012; Nakata & Snieder 2012; Wu & Peng 2012; Brenguier *et al.* 2014; Obermann *et al.* 2014; Richter *et al.* 2014; Gassenmeier *et al.* 2016) show that the seismic velocity of rocks is often reduced during shaking, and recovers afterwards. Gassenmeier *et al.* (2016) demonstrated that, at least in some cases, these changes are caused by the shaking of the subsurface that damages the material. Alternatively, static changes of the stress field have been thought to be the cause of transient velocity changes. The recovery process that returns the material properties to an equilibrium after a damaging event has been called *slow dynamics* (Ten Cate & Shankland 1996; Guyer & Johnson 2009) because high frequency shaking, or an instantaneous perturbation, causes a transient response of the seismic velocity. A similar behaviour is also observed in buildings, where the normal-mode frequencies or velocity of travelling waves is reduced after the building has been shaken by an earthquake (Clinton *et al.* 2006; Nakata *et al.* 2013, 2015). Because of the high accuracy (about 0.05 per cent) of measurements of velocity changes with coda waves (Poupinet *et al.* 1984; Snieder *et al.* 2002; Grêt *et al.* 2006; Hadziioannou *et al.* 2009), it is now possible to monitor time-lapse velocity changes in detail. Apart from changing the wave velocity, the shaking of rocks has also led to observed changes in the attenuation (Sato 1986, 1988).

The reduction in shear modulus due to shaking can contribute to triggering of earthquakes (Johnson & Jia 2005). The interplay between present and past deformation and friction properties has generated much interest because of its implication for triggering earthquakes. As a result, friction laws that are state- and rate-dependent have been applied to describe friction and slip on faults (Dieterich 1978, 1979; Ruina 1983; Heslot *et al.* 1994; Scholtz 1997). The imprint of deformation on the mechanical properties of rocks implies that the mechanics of rocks is, in general, nonlinear (Guyer & Johnson 2009; Rivière *et al.* 2013, 2015), and observations show that the seismic velocity and/or attenuation changes systematically with earth tides (Reasenberg & Aki 1974; Yamamura *et al.* 2003; Hillers *et al.* 2015). Because of the dominance of shear motion in strongly scattering elastic media (Aki & Chouet 1975; Weaver 1982; Snieder 2002), the measured change in arrival times of seismic waves corresponds for such media mostly to a change in shear velocity.

The recovery of the seismic velocity varies in many experiments logarithmically with time (Ten Cate *et al.* 2000; Johnson & Jia 2005;

Wu *et al.* 2009; Ten Cate 2011; Wu & Peng 2012; Gassenmeier 2015). A similar log-time dependence of relaxation has been observed for the slope of sandpiles that have been perturbed (Jaeger *et al.* 1988; Bocquet *et al.* 1998), numerical models for the slope of sandpiles (Duke *et al.* 1990), the compaction of granular media (Knight *et al.* 1995; Peng & Ohta 1998; Linz & Döhle 1999), slider-block models for earthquakes (Huisman & Fasolino 2006) and post-seismic deformation (Griggs 1939; Benioff 1951; Savage *et al.* 2005; Avouac 2015).

The macroscopic relaxation of materials that have been perturbed is, in general, due to a combination of different relaxation mechanisms on the microscopic scale. These mechanisms likely operate of different spatial and temporal scales. The healing rates of microcracks in quartz depend on the crack size (Brantley *et al.* 1990). Rock deformation depends on a variety of processes that include stress corrosion cracking, deposition, and pressure solution, these processes act on a variety of spatial and temporal scales and are temperature-dependent (Rutter 1976; Ojala *et al.* 2003; Kawada *et al.* 2006; Kay *et al.* 2006; Brantut *et al.* 2014). The formation and breaking of capillary bonds with different size within fractures have different activation energy, and therefore correspond to relaxation processes operating at different timescales (Bocquet *et al.* 1998). Observations of healing of cracks in gels reveal that the healing process takes place on different length and timescales, and that the distribution of healed parts of a fracture may have an intricate spatial organization (Renard *et al.* 2009).

On an intuitive level, one can understand the log-time behaviour of relaxation to imply that the relaxation does not operate on one specific timescale. Suppose the relaxation would depend on a timescale τ, then the time dependence would be given by $\ln(t/\tau) = \ln(t) - \ln(\tau)$. The relaxation time τ just shifts the relaxation with a constant: $\ln(t) \rightarrow \ln(t) - \ln(\tau)$, for this reason one can understand the log-time dependence to be due to the absence of only one specific relaxation time. A number of studies explain log-time relaxation by a superposition of different relaxation mechanisms that are associated with transitions of the system to states with a different energy (Gibbs *et al.* 1983; Shaknhovich & Gutin 1989; Ten Cate *et al.* 2000; Brey & Prados 2001; Amir *et al.* 2012; Zaitsev *et al.* 2014). It is thus established that relaxation that varies with the logarithm of time can be understood as the net result of the superposition of relaxation mechanisms with different relaxation times.

The logarithmic recovery poses, however, a conceptual problem, because when $t \rightarrow 0$ and as $t \rightarrow \infty$ the logarithm is infinite. The log-time relaxation model thus predicts that immediately after the perturbation ($t = 0$) and after a very long time ($t \rightarrow \infty$), the relaxation function, and hence the perturbed seismic velocity, diverges. This obviously cannot be the case, and the explanation of the relaxation must be modified to give a finite relaxation both for $t = 0$ and for very long time, while maintaining the log-time behaviour for intermediate times.

The purpose of this paper is to give a self-contained description of a relaxation function that (a) is consistent with observations in the sense that it varies logarithmically with time during most of relaxation process, (b) that is finite just after the perturbation ($t = 0$), (c) that approaches a finite value for very long time ($t \rightarrow \infty$), and (d) that is based on the Arrhenius model for the rate of chemical reactions. In contrast to earlier work (Brey & Prados 2001; Amir *et al.* 2012), we derive these properties without invoking the integral exponential function and its asymptotic properties. Our analysis does not rely on a waiting time t_w, as used by Amir *et al.* (2012), to make the short and long-time asymptotic behaviour finite.

We introduce the mathematical form of the relaxation model, along with numerical examples, in Section 2. In Section 3, we derive the properties of the relaxation function, including its behaviour for short and long times. We compare the behaviour of the relaxation model with a numerical simulation of a crude model for the closing of a fracture in Section 4, and describe the details of the fracture model in Appendix A. We propose in Section 5 that the behaviour of the relaxation function for long and short times may be a useful diagnostic to understand the healing process. The ubiquity of log-time relaxation suggests, just as the Gutenberg–Richter law does (Bak 1996), that the explanation of log-time relaxation does not depend on the details of the physics and chemistry that causes the relaxation, but that it is due to generic, or universal, properties of the relaxation process. We present the reasons for this universality in Section 6.

2 A MODEL FOR THE RELAXATION

We define a relaxation function $R(t)$ as a perturbation to a physical observable $O(t)$ of a system:

$$O(t) = O_0(1 + SR(t)), \tag{1}$$

where O_0 is the equilibrium value of O, and S a scale factor. The observable O might be the seismic velocity, an elastic modulus, the density of a granular material, or the electric or hydraulic conductivities.

The log-time relaxation is inconsistent with a relaxation mechanism that operates at one fixed relaxation time. In fact, a relaxation with a specific relaxation time τ corresponds to a relaxation function $\exp(-t/\tau)$, which obviously does not vary logarithmically with time. Following earlier work (Gibbs *et al.* 1983; Shaknhovich & Gutin 1989; Ten Cate *et al.* 2000; Brey & Prados 2001; Amir *et al.* 2012), we assume that a variety of relaxation processes are operative, and in this work we assume that the relaxation times are distributed between a minimum relaxation time $\tau_{\min}$ and a maximum relaxation time $\tau_{\max}$. The total relaxation is given by the following superposition of relaxation processes:

$$R(t) = \int_{\tau_{\min}}^{\tau_{\max}} \frac{1}{\tau} e^{-t/\tau} d\tau. \tag{2}$$

This relaxation function is dimensionless and must be scaled with expression (1) to describe time-dependent material properties. For example, when the velocity is perturbed at $t = 0$ from initial value v_0 to a reduced value $v_0 + \delta v$ with $\delta v < 0$, the relaxation is given by $v(t) = v_0 + \delta v R(t)/R(0)$. The normalization with $R(0)$ ensures that $v(t = 0) = v_0 + \delta v$.

The weight factor $1/\tau$ in the integrand can be justified from (1) the application of Arrhenius' law, (2) quantum mechanical tunnelling and (3) a product of relaxation processes operating of different timescales (Amir *et al.* 2012). Here we present the explanation based on Arrhenius' law (Gibbs *et al.* 1983; Amir *et al.* 2012). Suppose we have a relaxation process with activation energy E, then following Arrhenius' law (Laidler 1987), the corresponding relaxation time is given by

$$\tau = A \exp\left(\frac{E}{k_B T}\right), \tag{3}$$

with A a constant, T absolute temperature and k_B the Stephan–Boltzmann constant. Suppose the activation energy has a density of states $N(E)$, meaning that the number of activation mechanisms between E and $E + dE$ is equal to $N(E)dE$. The density of states

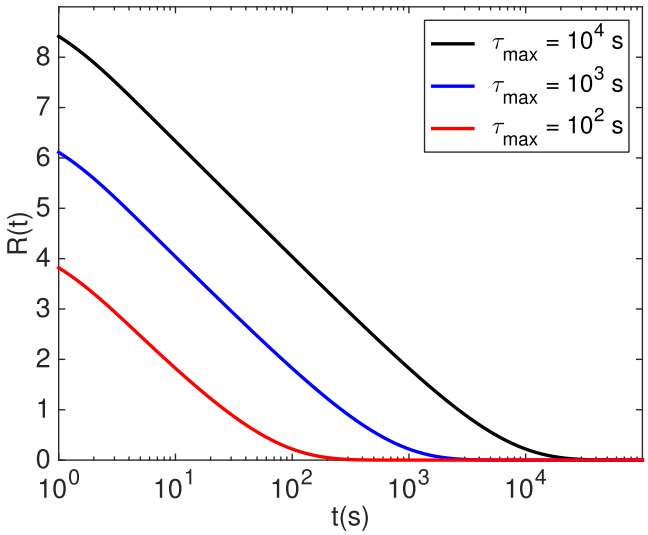

Figure 1. Relaxation function $R(t)$ for $\tau_{min} = 1\,s$ and $\tau_{max} = 10^4\,s$ (black), $\tau_{max} = 10^3\,s$ (blue) and $\tau_{max} = 10^2\,s$ (red).

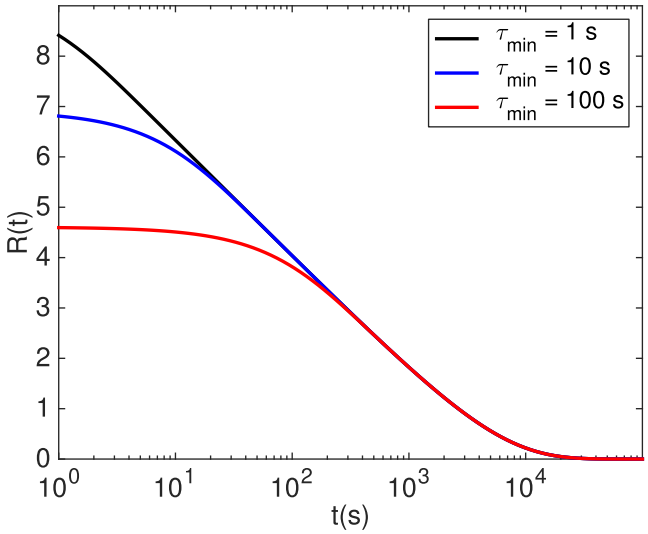

Figure 2. Relaxation function $R(t)$ for $\tau_{max} = 10^4\,s$ and $\tau_{min} = 1\,s$ (black), $\tau_{min} = 10\,s$ (blue) and $\tau_{min} = 100\,s$ (red).

$P(\tau)$ for the relaxation times satisfies $P(\tau) = N(E)dE/d\tau$. Using expression (3), $d\tau/dE = (A/k_BT)\exp(E/k_BT) = \tau/k_BT$, hence

$$P(\tau) = \frac{k_BT}{\tau}N(E). \tag{4}$$

When the distribution of the activation energy is uniform between a minimum activation energy E_{min} and maximum E_{max}, $N(E)$ is constant, and according expression (4) the density of states for a relaxation process with relaxation time τ is for a fixed temperature T proportional to $1/\tau$, which explains the $1/\tau$ dependence of the integrand of expression (2). Following expression (3), the minimum and maximum relaxation times are related to the minimum and maximum activation energies by

$$\tau_{min} = A\exp\left(\frac{E_{min}}{k_BT}\right), \quad \tau_{max} = A\exp\left(\frac{E_{max}}{k_BT}\right). \tag{5}$$

We show examples of the relaxation function in Figs 1 and 2 with time on a logarithmic scale along the horizontal axis. The curves are obtained by numerically evaluating the integral of expression (2). The curves in Fig. 1 decrease almost linearly up to a time $t \approx \tau_{max}$, and then flatten out. The relaxation thus is proportional to $\ln(t)$ for $t < \tau_{max}$. The maximum relaxation time τ_{max} can be inferred from relaxation curves by estimating the point where the logarithmic decay with time flattens off.

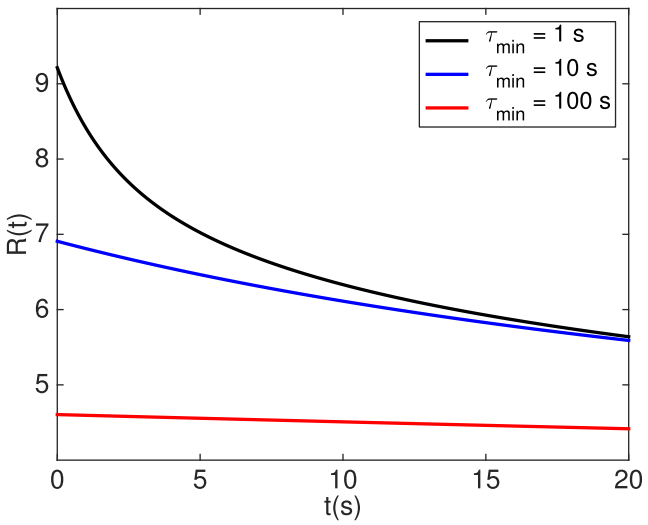

Figure 3. Relaxation function $R(t)$ for $\tau_{max} = 10^4\,s$ and $\tau_{min} = 1\,s$ (black), $\tau_{min} = 10\,s$ (blue) and $\tau_{min} = 100\,s$ (red) as a function of linear time.

The dependence of the relaxation function on the minimum relaxation time τ_{min} is shown in Fig. 2. In these examples the middle segment of the relaxation curves decays logarithmically with time, and for $t \approx 10^4\,s = \tau_{max}$ the relaxation functions flatten off. Note that the curves deviate from a logarithmic time dependence for $t < \tau_{min}$; the transition from the logarithmic dependence to the weaker log-time dependence at the left occurs at $t \approx \tau_{min}$, which suggests that τ_{min} can also be estimated from a given relaxation curve. One might infer from Fig. 2 that the relaxation curves are horizontal at $t = 0$. To show that this is not the case we show the same curves again in Fig. 3, but now with t on a linear scale. The curves clearly do not flatten near $t = 0$, and the slope increases for decreasing values of τ_{min}.

3 PROPERTIES OF THE RELAXATION FUNCTION

The integral in eq. (2) cannot be solved analytically, but when $t = 0$ the integral can be computed and is given by

$$R(0) = \ln(\tau_{max}/\tau_{min}). \tag{6}$$

Unlike a purely logarithmic relaxation, and in contrast to expression (1) of Amir *et al.* (2012) that was derived from the short-time limit of the logarithmic response to a perturbation over a time t_w, the relaxation function (2) is finite for $t = 0$.

To make the connection with $\ln(t)$ behaviour we change the integration variable in eq. (2) from τ into $u = t/\tau$, hence

$$R(t) = \int_{t/\tau_{max}}^{t/\tau_{min}} \frac{1}{u}e^{-u}\mathrm{d}u. \tag{7}$$

Taking the derivative with respect to t gives

$$\frac{\mathrm{d}R(t)}{\mathrm{d}t} = \frac{1}{t}\left(e^{-t/\tau_{min}} - e^{-t/\tau_{max}}\right). \tag{8}$$

To explain the logarithmic nature of the relaxation function we consider the case when $\tau_{min} \ll \tau_{max}$ and consider times t such that

$\tau_{\min} \ll t \ll \tau_{\max}$. In that case $e^{-t/\tau_{\min}} \approx 0$ and $e^{-t/\tau_{\max}} \approx 1$, which implies with eq. (8) that $\mathrm{d}R/\mathrm{d}t \approx -1/t$. Integrating this gives

$$R(t) \approx B - \ln(t) \text{ for } \tau_{\min} \ll \tau \ll \tau_{\max}, \tag{9}$$

with B an integration constant. The relaxation function $R(t)$ thus displays logarithmic behaviour, but only in a time interval bounded by the relaxation times. The slope of $R(t)$ versus $\ln(t)$ always is the same, as confirmed in figure 1, but this in only the case for a given normalization of $R(t)$. Multiplying the relaxation function with a scale factor S in eq. (1) multiplies of the logarithm in expression (9) with the same constant, and hence leads to a change in the slope of the relaxation versus $\ln(t)$.

The behaviour of $R(t)$ near $t = 0$ follows by making a Taylor expansion of the exponentials in eq. (8) and taking to limit $t \to 0$, this gives

$$\frac{\mathrm{d}R}{\mathrm{d}t}(t=0) = -\left(\frac{1}{\tau_{\min}} - \frac{1}{\tau_{\max}}\right). \tag{10}$$

With expression (6) the first-order Taylor series of $R(t)$ is thus given by

$$R(t) = \ln\left(\frac{\tau_{\max}}{\tau_{\min}}\right) - \left(\frac{1}{\tau_{\min}} - \frac{1}{\tau_{\max}}\right) t + O(t^2). \tag{11}$$

When $\tau_{\max} \gg \tau_{\min}$, the slope at $t = 0$ is approximately equal to $R'(t=0) \approx -1/\tau_{\min}$, and the ratio of the slope to $R(0)$ satisfies

$$\frac{|R'(0)|}{R(0)} \approx \frac{1/\tau_{\min}}{\ln(\tau_{\max}/\tau_{\min})}. \tag{12}$$

The maximum relaxation time $\tau_{\max}$ is the time by which the relaxation curve flattens out (see the numerical examples in Fig. 1). With this estimates of $\tau_{\max}$, expression (12) can then be used to estimate $\tau_{\min}$. Note that this procedure is independent of the normalization of the relaxation $R(t)$, that is, it can be applied directly to data.

The long-time behaviour of $R(t)$ follows by analysing expression (7) for the case $\tau_{\min} \ll \tau_{\max} \ll t$. In that case the upper limit of the integral can be replaced by ∞, so that

$$R(t) = \int_{t/\tau_{\max}}^{\infty} \frac{1}{u} e^{-u} \mathrm{d}u. \tag{13}$$

Using that $e^{-u} = -\mathrm{d}e^{-u}/\mathrm{d}u$ and applying integration by parts, reduces expression (13) to

$$R(t) = \frac{\tau_{\max}}{t} e^{-t/\tau_{\max}} - \int_{t/\tau_{\max}}^{\infty} \frac{1}{u^2} e^{-u} \mathrm{d}u. \tag{14}$$

The last integral satisfies

$$\int_{t/\tau_{\max}}^{\infty} \frac{1}{u^2} e^{-u} \mathrm{d}u \le \frac{\tau_{\max}^2}{t^2} \int_{t/\tau_{\max}}^{\infty} e^{-u} \mathrm{d}u = \frac{\tau_{\max}^2}{t^2} e^{-t/\tau_{\max}}, \tag{15}$$

hence

$$R(t) = \frac{\tau_{\max}}{t} e^{-t/\tau_{\max}} \left(1 + O\left(\frac{\tau_{\max}}{t}\right)\right). \tag{16}$$

Alternatively, one can apply integration by parts repeatedly to the right-hand side of expression (14) to derive an asymptotic series for $R(t)$. When the upper bound in expression (13) is not replaced by ∞, the same process of integration by parts can be applied and the right-hand side of expression (16) has an additional term $-(\tau_{\min}/t)e^{-t/\tau_{\min}}$. This term is, however, exponentially small, and the example of Fig. 2 shows that for $t \gg \tau_{\min}$ the relaxation function does not significantly depend on $\tau_{\min}$. Note the long-time behaviour predicted by expression (1) of Amir *et al.* (2012) does not include the exponential $\exp(-t/\tau_{\max})$. This is a consequence of the fact that their derivation of the long-time behaviour is, erroneously, based on the long-time limit of the logarithmic time behaviour.

If only the relaxation mechanism with the largest relaxation time $\tau_{\max}$ would contribute, the relaxation function would be equal to $R(t) = e^{-t/\tau_{\max}}$ instead of expression (16). The additional time dependence $\tau_{\max}/t$ in eq. (16) thus is due to relaxation mechanisms with relaxation time $\tau_{\min} < \tau < \tau_{\max}$. Since the time dependence of $1/t$ is slow compared to $e^{-t/\tau_{\max}}$ the relaxation is for large time approximately exponential.

The integrated relaxation function follows from expression (2)

$$\int_0^t R(t')\mathrm{d}t' = \int_0^t \int_{\tau_{\min}}^{\tau_{\max}} \frac{1}{\tau} e^{-t'/\tau} \mathrm{d}\tau \mathrm{d}t'. \tag{17}$$

Interchanging the integrations over t' and τ and carrying out the t'-integral gives

$$\int_0^t R(t')\mathrm{d}t' = \int_{\tau_{\min}}^{\tau_{\max}} \left(1 - e^{-t/\tau}\right) \mathrm{d}\tau. \tag{18}$$

As $t \to \infty$ the exponential vanishes, hence

$$\int_0^{\infty} R(t')\mathrm{d}t' = \tau_{\max} - \tau_{\min}. \tag{19}$$

Integrating measurements of $R(t)$ over time thus provides another constraint on $\tau_{\min}$ and $\tau_{\max}$.

Exponential relaxation is a special case of the general relaxation function (2), this is the case when $\tau_{\min}$ and $\tau_{\max}$ are close. Setting $\tau_{\min} = \tau_0 - \Delta$ and $\tau_{\max} = \tau_0 + \Delta$ gives to first order in Δ/τ_0:

$$R(t) = \frac{2\Delta}{\tau_0} e^{-t/\tau_0}, \tag{20}$$

and the relaxation function (2) in this case decays exponentially with time.

4 A CRUDE MODEL FOR A CLOSING FRACTURE

The relaxation function (2) is justified in this work on Arrhenius' law. Alternative justifications are quantum mechanical tunnelling, or a product of relaxation processes acting on different timescales (Amir *et al.* 2012). In this section, we present a model that satisfies neither of these criteria, but that follows the relaxation function (2) reasonably well. We use a crude model for a closing fracture, and have chosen this model because the healing of the seismic velocity might well be influenced by the closing of microcontacts in fractures. The closing of a fracture under an external load depends on the fracture topography (Greenwood & Williamson 1966; Brown & Scholz 1985a,b, 1986), a feature that is reproduced by our fracture model. The relation between fracture topography and the mechanical properties of fractures is not well understood, especially when there are mechanical interactions between different fractures.

Akin to earlier studies (Gangi 1978; Pyrak-Nolte & Morris 2000; Detwiler & Morris 2014) we describe a model for a closing fracture as a number of pillars, see Fig. 4. In contrast to these studies we simplify the model further by assuming that the pillars are placed on half spaces that do not deform. We assume that a constant normal stress σ compresses the pillars. The pillars themselves behave viscoelastically, and, as shown in Appendix A, the strain rate ε satisfies the following equation

$$\dot{\varepsilon} = -\frac{1}{n\eta}\left(N\sigma - \sum_{i,\text{closed}} \kappa \varepsilon_i\right), \tag{21}$$

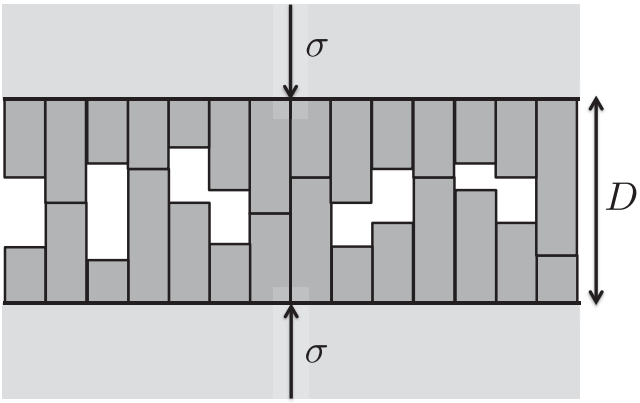

Figure 4. A model of pillars to describe the closing of a fracture.

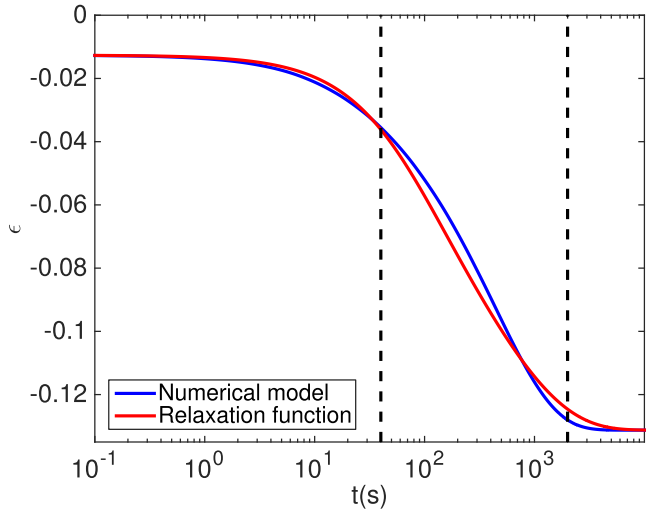

Figure 5. Numerically computed strain for a uniform distribution of pillar heights (blue) and scaled relaxation function (red). Dashed vertical lines denote $\tau_{\min} = 40$ s and $\tau_{\max} = 2000$ s, respectively.

where the overdot denotes a time derivative, N denotes the total number of pillars, n the number of closed pillars, κ the bulk modulus, and η the viscosity. The sum $\sum_{i,\,\text{closed}}$ is over all closed pillars. We integrate eq. (21) in time while keeping track of which pillars are touching. Note that the strain rate $\dot{\varepsilon}$ is the same for all touching pillars because they are placed between the same rigid half-spaces.

Our fracture model is extremely simple, and it is not meant to be an accurate description of a closing fracture. For example, we do not account for the shear stress between adjacent pillars. The pillar model violates a number of assumptions on which the relaxation model of Section 2 was based. The pillar model does not follow Arrhenius' law because the model does not include any thermally activated process. In addition, expression (2) presumes that the total relaxation is a superposition of relaxation mechanisms operating at different relaxation times τ. By contrast, our pillar model relaxes at any moment in time with only one fixed relaxation time that is determined by the fraction of pillars that touch at that moment; when few pillars touch the fracture is compressed rapidly, this compression slows down as more pillars touch an carry the load. The fracture model thus violates some of the assumptions on which the relaxation function (2) is based, but nevertheless relaxes in a way that is close to the relaxation function (2).

The strain in the pillar model computed by numerical integration of expression (21) is shown in Fig. 5 for a pillar distribution that

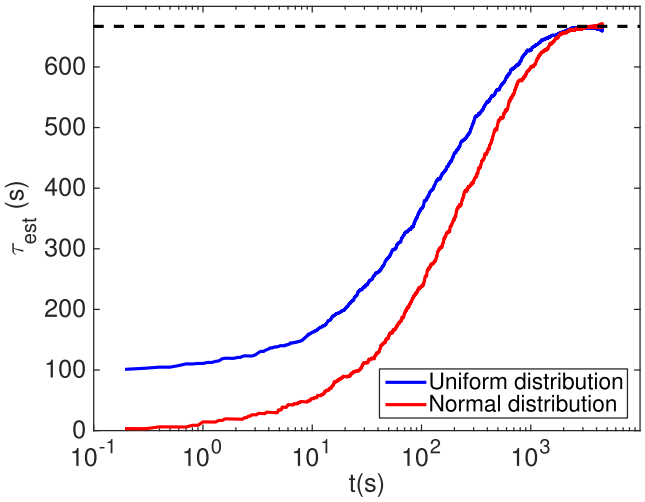

Figure 6. Estimated relaxation time τ_{est} as a function of time for the model with the uniform distribution of pillar height (blue line) and the model with normal distribution in pillar heights (red line). Dashed line shows the viscoelastic relaxation time $\tau_{\text{relax}} = \eta/\kappa = 667$ s.

initially is uniform with heights between 100 and 101. (Since only the strain is important, the unit used for the length of the pillar is not relevant.) The external stress is $\sigma = 5 \times 10^8$ Pa, $\kappa = 6 \times 10^{10}$ Pa and $\eta = 4 \times 10^{13}$ Pa s, and the time step in the numerical integration is $dt = 0.1$ s. Fig. 5 also shows a closely matching relaxation function $a + bR(t)$ for $\tau_{\min} = 40$ s and $\tau_{\max} = 2000$ s. The offset a and the scaling b account for the fact that the strain relaxes to a nonzero value for long times, and for the scaling of the relaxation function. We choose constants a and b so that the scaled relaxation function $a + bR(t)$ matches the strain at the last time sample ($t = 10^4$ s) and at the extrapolated value for $t = 0$.

The scaled relaxation function (2) matches the numerically computed relaxation reasonably well. This may be surprising, given the fact that the numerical model violates the assumptions on which the relaxation function is based. The agreement can be understood as follows. The pillar model relaxes at any moment in time with a characteristic relaxation time that is determined by the external load and the fraction of pillars that carry the load. As time progresses, more pillars carry the load, and the instantaneous relaxation time becomes longer. One can estimate the instantaneous relaxation time by evaluating

$$\tau_{\text{est}}(t) = -\frac{\varepsilon(t) - \varepsilon_\infty}{\dot{\varepsilon}(t)}, \tag{22}$$

where ε_∞ is the strain for very long time. The instantaneous relaxation time (blue curve in Fig. 6) increases from $\tau_{\text{est}} \approx 112$ s for early time to $\tau_{\text{est}} \approx 667$ s at late time. This produces a similar behaviour as a the superposition of relaxation mechanisms in expression (2), for early times the fast relaxation mechanism with relaxation time close to $\tau_{\min}$ dominate, while for late times the slow relaxation mechanism with relaxation time close to $\tau_{\max}$ contribute most.

The factor $1/\tau$ in the relaxation function (2) indicates that relaxation mechanisms with short time τ contribute more than slower relaxation mechanisms. The pillar model satisfies a similar dependence on the contribution of different relaxation mechanisms. At early times, few pillars touch, and the relaxation is rapid because the few pillars that touch deform rapidly. (The rapid relaxation at early times is not obvious in Fig. 5 because of the logarithmic timescale used in the plot, but the rate of change does decrease with linear time.) At late times more pillars touch, and as a result the relaxation

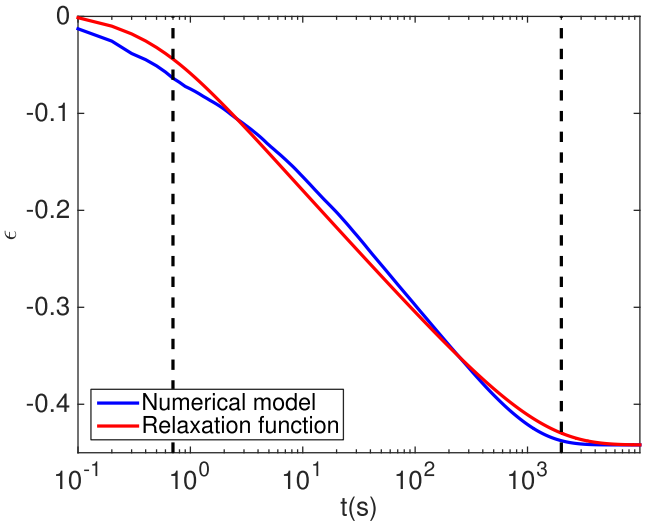

Figure 7. Numerically computed strain for a normal distribution of pillar heights with mean 1 and variance 0.5 (blue) and scaled relaxation function (red). Dashed vertical lines denote $\tau_{\min} = 0.7$ s and $\tau_{\max} = 2000$ s, respectively.

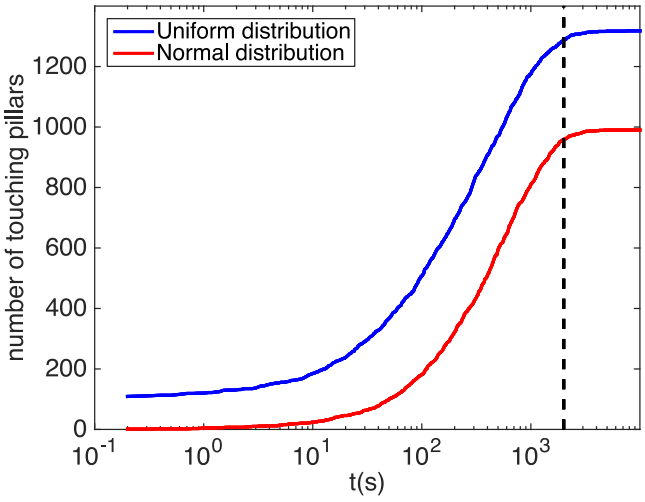

Figure 8. The number of touching pillars for the model with the uniform distribution of pillar height (blue line) and the model with normal distribution in pillar heights (red line). Dashed line shows $\tau_{\max} = 2000$ s.

is slow and the contribution to the compression is small. This results in a similar behaviour as the $1/\tau$ weighting in the relaxation function (2).

The relaxation of a fracture with a normal distribution of pillar heights can be described reasonably well with the relaxation function (2), but now for $\tau_{\min} = 0.7$ s and $\tau_{\max} = 2000$ s (Fig. 7). Note that in this case the relaxation is much more rapid than for the uniform distribution of pillar heights. The reason for the difference in the relaxation rate for early time can be understood by considering the number of touching pillars as shown in Fig. 8 for the uniform and the normal distribution of pillars. For the uniform pillar distribution, 109 pillars touch after the first time step. These pillars collectively carry the load, which results in a relatively slow relaxation. The normal distribution is known for its outliers, and for early times only a few pillars with an anomalously large height carry the load (Fig. 8). As a result the initial relaxation for the pillar model with a normal distribution of pillar heights is much more rapid than it is for the model with a uniform distribution of pillar heights. This rapid relaxation for the model with the normal distribution of pillar heights in confirmed in Fig. 6, which shows a much smaller instantaneous relaxation time $\tau_{\text{est}} \approx 3.2$ s at early times for the normal distribution than for the uniform distribution. Despite these differences in relaxation time, the relaxation is for both models approximated well by the relaxation function (2).

Note that the number of touching pillars for the uniform and normal distribution has a similar time dependence, both curves in Fig. 8 change at approximately the same rate. The time $\tau_{\max} = 2000$ s has the same value in the red relaxation curves in Figs 5 and 7. As shown in Fig. 8, this time corresponds to the time when the closing of pillars has come to an end and an equilibrium between the external stress and the static load carried by the pillars is reached.

5 RELAXATION AS A DIAGNOSTIC OF CHANGES IN SEISMIC VELOCITY

Relaxation of the seismic velocity after perturbing rocks has been observed in laboratory studies (Ten Cate & Shankland 1996; Zaitsev *et al.* 2003; Vakhnenko *et al.* 2004; Ten Cate 2011) and field observations (Poupinet *et al.* 1984; Schaff & Beroza 2004; Wegler & Sens-Schönfelder 2007; Brenguier *et al.* 2008; Wu *et al.* 2009; Nakata & Snieder 2011, 2012; Wu & Peng 2012; Brenguier *et al.* 2014; Obermann *et al.* 2014; Richter *et al.* 2014), and is thus an observable property under the right conditions. These observations usually show a recovery similar to the relaxation shown in Fig. 1 that varies logarithmically with time, until the recovery stops. This can be described by the relaxation function (2). The numerical experiments of Figs 5–7 show that, for the pillar model of a closing fracture, the relaxation depends on the statistical distribution of the fracture roughness. In general, the relaxation depends on the distribution of relaxation processes acting on different timescales, which in many cases correspond to relaxation processes operating on different spatial scales. The relaxation function can therefore be a diagnostic for the temporal and spatial distribution of healing processes.

The relaxation function (2) may suffice for many observations of relaxation, but for a general distribution $P(\tau)$ of relaxation times the relaxation function can be written as

$$R(t) = \int_0^\infty P(\tau) e^{-t/\tau} \mathrm{d}\tau. \tag{23}$$

Such a general superposition of relaxation processes has been proposed for induced polarization (Morgan & Lesmes 1994), nuclear magnetic resonance (NMR; Whittall & MacKay 1989), and rock deformation (Kawada *et al.* 2006). When $P(\tau)$ is not proportional to $1/\tau$, the relaxation satisfies a power-law instead of a logarithmic time dependence (Cole & Cole 1941; Morgan & Lesmes 1994). Such a power-law dependence has been proposed for long-term rock deformation (Main 2000; Kawada *et al.* 2006).

The distribution $P(\tau)$ of relaxation times from the observed relaxation function $R(t)$ can be estimated in different ways. First, as shown in Figs 5 and 7 one can estimate $\tau_{\min}$ and $\tau_{\max}$ by fitting the observed relaxation to the relaxation function (2). Alternatively, one can gain an impression of the spread of relaxation times by computing τ_{est} using expression (22), an example of this is shown in Fig. 6. Second, by making the substitution $\tau = 1/s$, one can write eq. (23) as $R(t) = \int_0^\infty F(s) e^{-st} \mathrm{d}s$, with $F(s) = s^{-2} P(1/s)$. The relaxation function can thus be written as a Laplace transform, and one can find P using an inverse Laplace transform (Davies & Martin 1979; Abate & Whitt 1995; Kuhlman 2013). Third, one can view expression (23) as a linear inverse problem to estimate $P(\tau)$ given

$R(t)$. In that approach techniques of linear inversion (Menke 1984; Tarantola 1987; Aster *et al.* 2004) can be utilized to estimate the distribution of relaxation times $P(\tau)$. Methods for estimating relaxation spectra are an essential part for interpreting measurements of induced polarization (Morgan & Lesmes 1994; Tong *et al.* 2006; Tarasov & Titov 2007) and NMR (Whittall & MacKay 1989). In NMR the relaxation time may, in fact, depend on location (Blümich 2000).

We applied the first approach, estimation of $\tau_{\min}$ and $\tau_{\max}$ to the fracture model. For the pillar with the uniform distribution of pillar height (Fig. 5), $\tau_{\min} = 40$ s and $\tau_{\max} = 2000$ s. (Note that the fit of the relaxation curve in Fig. 5 is not perfect). The spread of estimated instantaneous relaxation times τ_{est} from 101 to 667 s, shown in Fig. 6, is of the same order of magnitude as $\tau_{\min}$ and $\tau_{\max}$, respectively. But Fig. 6 shows that the largest instantaneous relaxation time is explained well by the viscoelastic relaxation time $\eta/\kappa = 667$ s of the pillars, rather than $\tau_{\max} = 2000$ s. The reason for this discrepancy is that the relaxation in the pillar model does not satisfy the relaxation function (2) in its details. As shown in Fig. 5 the pillar model relaxes more slowly for late times than the relaxation function (2) predicts. Such discrepancies can be an indication to seek a relaxation function (23) with a more general distribution function $P(\tau)$ of relaxation times than the relaxation function (2).

In realistic observations of the relaxation of the seismic velocity of Earth materials, the relaxation function (2) may adequately explain the observations within the experimental uncertainties. In that case one may hope to retrieve the minimum and maximum relaxation times $\tau_{\min}$ and $\tau_{\max}$. What do these times say in general about relaxation mechanisms? The minimum relaxation time $\tau_{\min}$ is related to the relaxation mechanism on the smallest scale. This could be the nanoscale, or even the atomic scale. Observed post-seismic velocity variations show a logarithmic relaxation as a function of time from the earliest measurement (Wu *et al.* 2009; Wu & Peng 2012), which indicates that the shortest relaxation mechanism operates on a time less than the smallest observation time. The minimum relaxation time $\tau_{\min}$ can, however, not be equal to zero, because the integral (6) diverges for $\tau_{\min} = 0$. The longest relaxation time $\tau_{\max}$ is the time where the relaxation stops (e.g. Fig. 1). Observations of this equilibration time range from about 100 s for the M_{W} 6.6 mid-Niigata earthquake sequence (Wu *et al.* 2009), to about 10 d for the M_{W} Tohoku-Oki earthquake (Wu & Peng 2012), to about 2–3 yr for the M_{W} Parkfield earthquake (Brenguier *et al.* 2008). The maximum relaxation time $\tau_{\max}$ depends in an as yet unknown way on the initial perturbation (such as the shaking that causes slow dynamics), the ambient stress, temperature and fluid content, and the depth at which the velocity is perturbed. It may be a useful diagnostic of the physics and/or chemistry of the relaxation process.

6 CONCLUSIONS

The relaxation function (2) explains the logarithmic relaxation that is observed in laboratory experiments and field observations of earth materials, and is finite just after the perturbation $t = 0$ and for long times $t \to \infty$. Although the relaxation function (2) can be explained by Arrhenius law, quantum mechanical tunnelling, and a product of relaxation processes (Amir *et al.* 2012), it is applicable to other models as well. The pillar model is an example of a model that does not satisfy either of these assumptions, but that fits the relaxation (2) reasonably well. Sandpiles and compacting granular media have grains that are too heavy to be influenced by thermal motion (Jaeger & Nagel 1992) or by quantum mechanical tunnelling, yet such systems display relaxation that varies logarithmically in time as well. The ubiquity of logarithmic relaxation suggests a universal behaviour of the relaxation function. The essential elements of the relaxation function (2) and the pillar model are listed below:

(i) At different times different relaxation mechanisms dominate. In the pillar model the relaxation time as the number of pillars that touch changes (Fig. 6) while in the relaxation law (2) contributions $e^{-t/\tau}$ do effectively not contribute when $t \gg \tau$.

(ii) The effective relaxation time increases with time.

(iii) The faster relaxation mechanisms (small τ) give a larger contribution to the relaxation than the slower relaxation mechanisms. The pillar model is compressed much when few pillars touch, while in the relaxation function (2) the term $1/\tau$ gives a greater weight to fast relaxation processes.

(iv) Beyond a maximum relaxation time no relaxation mechanisms contribute. This time depends on the perturbation that triggers the relaxation and ambient conditions such as pressure, temperature and chemistry.

(v) Below a minimum relaxation time there are no relaxation processes that contribute. This minimum relaxation time may be so small that it not observable.

The properties listed above are general characteristics of multiscale relaxation phenomena. This explains the ubiquity of the observed log-time behaviour in slow dynamics. The relaxation law (2) does not necessarily give an accurate description of the distribution of relaxation times, and the relative contribution of the relaxation operating at different relaxation times. In that case the relaxation function (2) can be extended to the more general relaxation law (23). Given an observed relaxation function $R(t)$, and can apply linear inverse theory to estimate the density $P(\tau)$ of relaxation mechanisms as a function of τ.

In practice, the relaxation function (2) may suffice to explain observations of relaxation. The shortest and longest relaxation times $\tau_{\min}$ and $\tau_{\max}$ may be inferred from observations of the relaxation. Measurements of $\tau_{\min}$ potentially give information on the fastest relaxation mechanism, which is likely related to the relaxation process that takes place on the smallest spatial scale. Since that scale can be very small, it may not be possible to obtain reliable measurements of $\tau_{\min}$. Measuring the dependence of $\tau_{\max}$ as a function of the strength of the perturbation and ambient parameters such as pressure and temperature is a potentially useful diagnostic of healing mechanisms. It may be especially interesting to combine macroscopic observations of the healing of rocks with measurements of the micro-structure of these materials.

ACKNOWLEDGEMENTS

We thank Georg Dresen, Ian Main, Jörg Renner and an anonymous reviewer for their critical and constructive comments.

REFERENCES

Abate, J. & Whitt, W., 1995. Numerical inversion of Laplace transforms of probability functions, *ORSA J. Comput.,* **7**(1), 36–43.

Aki, K. & Chouet, L., 1975. Origin of coda waves: source, attenuation, and scattering effects, *J. geophys. Res.,* **80,** 3322–3342.

Amir, A., Oreg, Y. & Imry, Y., 2012. On relaxations and aging of various glasses, *Proc. Natl. Acad. Sci. USA,* **109,** 1850–1855.

Aster, R., Borchers, B. & Thurber, C., 2004. *Parameter Estimation and Inverse Problems,* Academic Press.

Avouac, J.P., 2015. From geodetic imaging of seismic and aseismic fault slip to dynamic modelling of the seismic cycle, *Annu. Rev. Earth Planet. Sci.,* **43,** 233–271.

Bak, P., 1996. *How Nature Works,* Copernicus.

Benioff, H., 1951. Earthquakes and rock creep, *Bull. seism. Soc. Am.,* **41,** 31–62.

Blümich, B., 2000. *NMR Imaging of Materials,* Clarendon Press.

Bocquet, L., Charlaix, E., Ciliberto, S. & Crassous, 1998. Moisture-induced ageing in granular media and the kinetics of capillary condensation, *Nature,* **396,** 735–737.

Brantley, S., Evans, B., Hickman, S. & Crerar, D., 1990. Healing of microcracks in quartz: implications for fluid flow, *Geology,* **18,** 136–139.

Brantut, N., Heap, M., Baud, P. & Meredith, P., 2014. Mechanisms of time-dependent deformation in porous limestone, *J. geophys Res.,* **119,** 5444–5463.

Brenguier, F., Campillo, M., Hadziioannou, C., Shapiro, N. & Larose, E., 2008. Postseismic relaxation along the San Andreas Fault at Parkfield from continuous seismological observations, *Science,* **321,** 1478–1481.

Brenguier, F., Campillo, M., Takeda, T., Aoki, Y., Shapiro, N., Briand, X., Emoto, K. & Miyake, H., 2014. Mapping pressurized volcanic fluids from induced crustal seismic velocity drops, *Science,* **345,** 80–82.

Brey, J. & Prados, A., 2001. Slow logarithmic relaxation in models with hierarchically constrained dynamics, *Phys. Rev. E,* **63,** 021108, doi:10.1103/PhysRevE.63.021108.

Brown, S. & Scholz, C., 1985a. Closure of random elastic surfaces in contract, *J. geophys. Res.,* **90,** 5531–5545.

Brown, S. & Scholz, C., 1985b. Broad bandwidth of the topography of natural rock surfaces, *J. geophys. Res.,* **90,** 12 575–12 582.

Brown, S. & Scholz, C., 1986. Closure of rock joints, *J. geophys. Res.,* **91,** 4939–4948.

Clinton, J., Case Bredford, S., Heaton, T. & Favela, J., 2006. The observed wander of the natural frequencies in a structure, *Bull. seism. Soc. Am.,* **96,** 237–257.

Cole, K. & Cole, R., 1941. Dispersion and absorption in dielectrics: I. Alternating current characteristics, *J. Chem. Phys.,* **9,** 341–352.

Davies, B. & Martin, B., 1979. Numerical inversion of the Laplace transform: a survey and comparison of methods, *J. Comput. Phys.,* **33**(1), 1–32.

Detwiler, R. & Morris, J., 2014. Transmissivity anisotropy in rough-walled fractures: the combined influence of shear offset and normal deformation, in *Proc. 48th US Rock Mechanics/Geomechanics Symposium,* Minneapolis, MN, 1–4 June 2014, pp. 14–7539, American Rock Mechanics Association.

Dieterich, J., 1978. Time-dependent friction and the mechanics of stick slip, *Pure appl. Geoph.,* **116,** 790–806.

Dieterich, J., 1979. Modeling of rock friction. 1: Experimental results and constitutive equations, *J. geophys. Res.,* **84,** 2161–2168.

Duke, T., Barker, G. & Mehta, A., 1990. A Monte Carlo study of granular relaxation, *Europhys. Lett.,* **13,** 19–24.

Gangi, A., 1978. Variation of whole and fractured porous rock permeability with confining pressure, *Int. J. Rock Mech. Min. Sci.,* **15,** 249–257.

Gassenmeier, M., 2015. Observation of dynamic processes with seismic interferometry, *PhD thesis,* Universität Leipzig.

Gassenmeier, M., Sens-Schönfelder, C., Eulenfeld, T., Bartsch, M., Victor, P., Tilmann, F. & Korn, M., 2016. Field observations of seismic velocity changes caused by shaking-induced damage and healing due to mesoscopic nonlinearity, *Geophys. J. Int.,* **204**(3), 1490–1502.

Gibbs, M., Evetts, J. & Leake, J., 1983. Activation energy spectra and relaxation in amorphous materials, *J. Mater. Sci.,* **18,** 278–288.

Greenwood, J. & Williamson, J., 1966. Contact of nominally flat surfaces, *Proc. R. Soc. A,* **295,** 300–319.

Grêt, A., Snieder, R. & Scales, J., 2006. Time-lapse monitoring of rock properties with coda wave interferometry, *J. geophys. Res.,* **111,** B03305, doi:10.1029/2004JB003354.

Griggs, D., 1939. Creep of rocks, *J. Geol.,* **47,** 225–251.

Guyer, R. & Johnson, P., 2009. *Nonlinear Mesoscopic Elasticity,* Wiley-VCH.

Hadziioannou, C., Larose, A., Coutant, O., Roux, P. & Campillo, M., 2009. Stability of monitoring weak changes in multiply scattering media with ambient noise correlation: laboratory experiments, *J. acoust. Soc. Am.,* **125,** 3688–3695.

Heslot, F., Baumberger, T., Perrin, B., Caroli, B. & Caroli, C., 1994. Creep, stick-slip, and dry-friction dynamics: experiments and a heuristic model, *Phys. Rev. E,* **49,** 4973–4988.

Hillers, G., Retailleau, L., Campillo, M., Inbal, A., Ampuero, J.-P. & Nishim, 2015. In situ observations of velocity changes in response to tidal deformation of the high-frequency ambient wavefield, *J. geophys. Res.,* **120,** 210–225.

Hobiger, M., Wegler, U., Shiomi, K. & Nakahara, H., 2012. Coseismic and postseismic elastic wave velocity variations caused by the 2008 Iwate-Miyagi Nairiku earthquake, Japan, *J. geophys. Res.,* **117**(B9), 1–19.

Huisman, B. & Fasolino, A., 2006. Logarithmic relaxation due to minimization of interactions in the Burridge-Knopoff model, *Phys. Rev. E,* **74,** 026110, doi:10.1103/PhysRevE.74.026110.

Jaeger, H. & Nagel, S., 1992. Physics of the granular state, *Science,* **255,** 1523–1531.

Jaeger, H., Liu, C. & Nagel, R., 1988. Relaxation at the angle of repose, *Phys. Rev. Lett.,* **62,** 40–43.

Johnson, P. & Jia, X., 2005. Nonlinear dynamics, granular media and dynamic earthquake triggering, *Nature,* **437,** 871–874.

Kawada, Y., Nagahama, H. & Hara, H., 2006. Irreversible thermodynamic and viscoelastic model for power-law relaxation and attenuation of rocks, *Tectonophysics,* **427,** 255–263.

Kay, M., Main, I., Elphick, S. & Ngwenya, B., 2006. Fault gauge diagenesis at shallow burial depth: solution-precipitation reactions in well-sorted and poorly sorted powders of crushed sandstone, *Earth planet. Sci. Lett.,* **243,** 607–614.

Knight, J., Fandrich, C., Lau, C., Jaeger, H. & Nagel, S., 1995. Density relaxation in a vibrated granular material, *Phys. Rev. E,* **51,** 3957–3963.

Kuhlman, K., 2013. Review of inverse Laplace transform algorithms for Laplace-space numerical approaches, *Numer. Algorithms,* **63,** 339–355.

Laidler, K., 1987. *Chemical Kinetics,* 3rd edn, Haper & Row.

Linz, S. & Döhle, A., 1999. Minimal relaxation law for compaction of tapped granular matter, *Phys. Rev. E,* **60,** 5737–5741.

Main, I., 2000. A damage mechanics model for power-law creep and earthquake aftershocks and foreshocks sequences, *Geophys. J. Int.,* **142,** 151–161.

Menke, W., 1984. *Geophysical Data Analysis: Discrete Inverse Theory,* Academic Press.

Morgan, F. & Lesmes, D., 1994. Inversion for dielectric relaxation spectra, *J. Chem. Phys.,* **100,** 671–681.

Nakata, N. & Snieder, R., 2011. Near-surface weakening in Japan after the 2011 Tohoku-Oki earthquake, *Geophys. Res. Lett.,* **38,** L17302, doi:10.1029/2011GL048800.

Nakata, N. & Snieder, R., 2012. Estimating near-surface shear-wave velocities in Japan by applying seismic interferometry to KiK-net data, *J. geophys. Res.,* **117,** B01308, doi:10.1029/2011JB008595.

Nakata, N., Snieder, R., Kuroda, S., Ito, S., Aizawa, T. & Kunimi, T., 2013. Monitoring a building using deconvolution interferometry. I: Earthquake-data analysis, *Bull. seism. Soc. Am.,* **103,** 1662–1678.

Nakata, N., Tanaka, W. & Oda, Y., 2015. Damage detection of a building casued by the 2011 Tohoko-Oki earthquake with seismic interferometry, *Bull. seism. Soc. Am.,* **105,** 2411–2419.

Obermann, A., Froment, B., Campillo, M., Larose, E., Planès, T., Valette, B., Chen, J. & Liu, Q., 2014. Seismic noise correlations to image structural and mechanical changes associated with the Mw 7.9 2008 Wenchuan earthquake, *J. geophys. Res.,* **119,** 3155–3168.

Ojala, I., Ngwenya, B., Main, I. & Elphick, S., 2003. Correlation of microseismic and chemical properties of brittle deformation in Locharbriggs sandstone, *J. gephys. Res.,* **108,** 2268, doi:10.1029/2002JB002277.

Peng, G. & Ohta, T., 1998. Logarithmic density relaxation in compaction of granular materials, *Phys. Rev. E.,* **57,** 829–833.

Poupinet, G., Ellsworth, W. & Fréchet, J., 1984. Monitoring velocity variations in the crust using earthquake doublets: an application to the Calaveras Fault, California, *J. geophys. Res.,* **89,** 5719–5731.

Pyrak-Nolte, L. & Morris, J., 2000. Single fractures under normal stress: The relation between fracture specific stiffness and fluid flow, *Int. J. Rock Mech. Min. Sci.,* **37,** 245–262.
Reasenberg, P. & Aki, K., 1974. A precise continuous measurement of seismic velocity for monitoring in situ stress, *J. geophys. Res.,* **79,** 399–406.
Renard, F., Dysthe, D., Feder, J., Meakin, P., Morris, S. & Jamtveit, B., 2009. Pattern formation during healing of fluid-filled cracks: an analog experiment, *Geofluids,* **9,** 365–372.
Richter, T., Sens-Schönfelder, C., Kind, R. & Asch, G., 2014. Comprehensive observation and modeling of earthquake and temperature-related seismic velocity changes in northern Chile with passive image interferometry, *J. geophys. Res.,* **119,** 4747–4765.
Rivière, J., Renaud, G., Guyer, R. & Johnson, P., 2013. Pump and probe waves in dynamic acousto-elasticity: comprehensive description and comparison with nonlinear elastic theories, *J. Appl. Phys.,* **114,** 054905, doi:10.1063/1.4816395.
Rivière, J., Skokouhi, P., Guyer, R. & Johnson, P., 2015. A set of measurements for the systematic classification of the nonlinear elastic behavior of disparate rocks, *J. geophys. Res.,* **120,** 1587–1604.
Ruina, A., 1983. Slip instability and state variable friction laws, *J. geophys. Res.,* **88,** 10 359–10 370.
Rutter, E., 1976. The kinetics of rock deformation by pressure solution, *Phil. Trans. R. Soc. Lond., A,* **283,** 203–219.
Sato, H., 1986. Temporal change in attenuation intensity before and after the eastern Yamanashi earthquake of 1983 in Central Japan, *J. geophys. Res.,* **91,** 2049–2061.
Sato, H., 1988. Temporal change in scattering and attenuation associated with the earthquake occurrence - a review of recent studies on coda waves, *Pure appl. Geophys.,* **126,** 465–497.
Savage, J., Svarc, J. & Yu, S.-B., 2005. Postseismic relaxation and transient creep, *J. geophys. Res.,* **110,** B11402, doi:10.1029/2005JB003687.
Schaff, D. & Beroza, G., 2004. Coseismic and postseismic velocity changes measured by repeating earthquakes, *J. geophys. Res.,* **109,** B10302, doi:10.1029/2004JB003011.
Scholtz, C., 1997. Earthquakes and friction laws, *Nature,* **391,** 37–42.
Shaknhovich, E. & Gutin, A., 1989. Relaxation to equilibrium in the random energy model, *Europhys. Lett.,* **9,** 569–574.
Snieder, R., 2002. Coda wave interferometry and the equilibration of energy in elastic media, *Phys. Rev. E,* **66,** 046615, doi:10.1103/PhysRevE.66.046615.
Snieder, R., Grêt, A., Douma, H. & Scales, J., 2002. Coda wave interferometry for estimating nonlinear behavior in seismic velocity, *Science,* **295,** 2253–2255.
Tarantola, A., 1987. *Inverse Problem Theory,* Elsevier.
Tarasov, A. & Titov, K., 2007. Relaxation time distribution from time domain induced polarization measurements, *Geophys. J. Int.,* **170,** 31–43.
Ten Cate, J., 2011. Slow dynamics of earth materials: an experimental overview, *Pure appl. Geoph.,* **168,** 2211–2219.
Ten Cate, J.A. & Shankland, T.J., 1996. Slow dynamics in the nonlinear elastic response of Berea sandstone, *Geophys. Res. Lett.,* **21,** 3019–3022.
Ten Cate, J., Smith, E. & Guyer, R., 2000. Universal slow dynamics in granular solids, *Phys. Rev. Lett.,* **85,** 1020–1023.
Tong, M., Li, L., Wang, W. & Jiang, Y., 2006. Determining capillary-pressure curve, pore-size distribution, and permeability from induced polarization of shaley sand, *Geophysics,* **71,** N33–N40.
Vakhnenko, O., Vakhnenko, V., Shankland, T. & Ten Cate, J., 2004. Strain-induced kinetics of intergrain defects as the mechanism of slow dynamics in the nonlinear resonant response of humid sandstone bars, *Phys. Rev. E,* **70,** 015602(R), doi:10.1103/PhysRevE.70.015602.
Weaver, R., 1982. On diffuse waves in solid media, *J. acoust. Soc. Am.,* **71,** 1608–1609.
Wegler, U. & Sens-Schönfelder, C., 2007. Fault zone monitoring with passive image interferometry, *Geophys. J. Int.,* **168,** 1029–1033.
Whittall, K. & MacKay, A., 1989. Quantitative interpretation of NMR relaxation data, *J. Magn. Reson.,* **84,** 134–152.
Wu, C. & Peng, Z., 2012. Long-term change of the site response after the M_w 9.0 Tohoku earthquake in Japan, *Earth Planets Space,* **64,** 1259–1266.
Wu, C., Peng, Z. & Assimaki, D., 2009. Temporal changes in site response associated with the strong ground motion of the 2004 m_w 6.6 Mid-Niigata earthquake sequences in Japan, *Bull. seism. Soc Am.,* **99,** 3487–3495.
Yamamura, K., Sano, O., Utada, H., Takei, Y., Nakao, S. & Fukao, Y., 2003. Long-term observations of in situ seismic velocity and attenuation, *J. geophys. Res.,* **108**(B6), doi:10.1029/2002JB002005.
Zaitsev, V., Gusev, V. & Castagnede, B., 2003. Thermoelastic mechanism for logarithmic slow dynamics and memory in elastic wave interactions with individual cracks, *Phys. Rev. Lett.,* **90,** 075501, doi:10.1103/PhysRevLett.90.075501.
Zaitsev, V., Gusev, V., Tournat, V. & Richard, P., 2014. Slow relaxation and aging phenomena at the nanoscale in granular materials, *Phys. Rev. Lett.,* **112,** 108302, doi:10.1103/PhysRevLett.112.108302.

APPENDIX A: THE PILLAR MODEL OF THE CLOSING FRACTURE

We describe in this section the dynamics of the pillar model of Fig. 4. The pillars at the top and the bottom of the fracture may have different length, but once they touch the normal stress in these pillars is the same, and therefore the strain in pillars that touch is equal too. The subscript i refers to the pillars. Since the strain in the top and bottom pillars is the same, the only relevant quantity to monitor is the combined height h_i of each pair of top and bottom pillars. When the strain rate $\dot{\varepsilon}$ is known, the time evolution of the pillar height and the distance between the half spaces can be computed, because the pillar height satisfies

$$\frac{\partial h_i}{\partial t} = \dot{\varepsilon} h_i, \tag{A1}$$

and the distance D between the half spaces, as defined in Fig. 4, satisfies the same equation

$$\frac{\partial D}{\partial t} = \dot{\varepsilon} D. \tag{A2}$$

The strain rate can also be used to update the strain in the pillars that touch.

When the pillars behave viscoelastically, the stress σ_i in each pillar is related to the strain by

$$\sigma_i = \kappa \varepsilon_i + \eta \dot{\varepsilon}, \tag{A3}$$

where we used that the pillars are placed on rigid half-spaces, and hence the strain rate in all pillars that touch is identical. The stress carried by the pillars, the left hand side of expression (A3), is balanced by the external normal stress σ:

$$\sum_{i,\text{closed}} (\kappa \varepsilon_i + \eta \dot{\varepsilon}) = -N\sigma, \tag{A4}$$

where $\sum_{i,\text{closed}}$ is a sum over all pillars that touch, and N is the total number of pillars. The minus sign accounts for the fact that for a compressive stress, the pillars shorten, which corresponds to $\varepsilon < 0$. Solving eq. (A4) for the strain rate gives

$$\dot{\varepsilon} = -\frac{1}{n\eta}\left(N\sigma - \sum_{i,\text{closed}} \kappa \varepsilon_i\right), \tag{A5}$$

where n is the number of pillars that touch.

The closing of the fracture can be modelled by using eq. (A5) to compute the strain rate. For a given strain rate, the change in the distance D can be computed using expression (A2). With this update in D it can be determined if new pillars close. The change in pillar height can be computed from expression (A1). This gives the updated strain ε_i in each pillar, which can be used to compute the new strain rate with eq. (A5).